68th International Astronautical Congress (IAC), Adelaide, Australia, 25-29 September 2017.

IAC-17,A4,1,10,x37503

Exploring Optical SETI's Middle Ground

Richard H. Stanton

Jet Propulsion Laboratory (retired) 1429 Shay Road, Big Bear City, CA, USA 92314 rhstanton@gmail.com

Abstract

The Search for Extra-Terrestrial Intelligence (SETI) in optical wavelengths has recently concentrated either on detecting intense short light pulses that briefly outshine the background star, or on finding unique spectral features that stand out in a star's spectrum. But there is a middle ground available where the temporal variation of an optical SETI source would distinguish it from its stellar background. Initial results are presented for frequency-domain searches, covering a signal range of 1 to 10,000Hz, with an instrument that simultaneously measures two broad optical spectral bands. It is shown that signals a thousand times fainter than the background starlight can be detected using this instrument coupled to a meter-class telescope. This limit can be extended further with a larger telescopes and more capable instruments. **Keywords:** Photon counting, periodic optical signals, power spectra

Acronyms/Abbreviations

Extraterrestrial Intelligence (ETI)–noun or adjective;
Fast Fourier Transform (FFT);
Photo Multiplier Tube (PMT);
Relative Signal Amplitude (RSA), the peak-to-peak amplitude of a signal divided by the host star brightness (both in photon counts per sample);
Spectral Signal to Noise Ratio (SSNR), amplitude of a detected peak in the power spectrum divided by the background RMS noise in that spectrum (both in dB).

1. Introduction

The search for ETI signals has been underway for roughly 60 years. While early activity concentrated on radio wavelengths [1], it was soon demonstrated that searches in the optical spectrum could also be justified [2]. This presented researchers with a broad electromagnetic spectrum to explore. Since those early days, searches have continued with greatly improved sensitivity and expanded wavelength coverage [3-5].

Searches in optical wavelengths can use many different approaches and instruments, based primarily on assumptions of expected signal characteristics. At least four distinct signal types can be identified:

Type I Short, ***high intensity pulses*** of visible or infrared photons can be sought that briefly (nanoseconds) outshine the ETI host star. Searches for such signals make sense since we ourselves have the capability of generating similar fast (laser) pulses. It can be shown that ETI using our current level of technology could generate optical bursts that outshine the host star by as much as four orders of magnitude [6]. Since the discovery of such a signal would be difficult to explain as a natural phenomenon, any confirmed detection would be considered a strong indication of intelligent activity. This fact has inspired a number of investigators to look for fast pulses in both optical and infrared wavelengths [4, 6-9].

Type II A second approach searches ***optical spectra*** for any sign of unexplained structure, such as an unusual or an emission physically close to a star that might possibly come from an orbiting planet. An unusual spectral feature might be generated by a laser or ETI actions stimulating unexpected emission or absorption in the parent star or its surroundings [10, 11]. A related search for spectral evidence optical pulse trains of picosecond separation has been suggested [12].

Type III A third approach searches for optical signals intentionally ***modulated*** by extraterrestrials. In a sense, this represents a middle ground between Type I and Type II, since a signal undetectable as either a fast pulse or obvious spectral feature might be detected by its variability. Searches for repeating optical pulses fall into this category [4, 13]. While individual pulses may not be identified as extraterrestrial, their recurrence at regular intervals could be decisive. A more general approach would be to search for evidence of ***any repeating waveform..*** The source of this signal could be a laser beamed intentionally toward Earth, or even a white-light signal generated by modulation of the home star's light[14].

Type IV This final category includes all other types of optical signal not included in Types I-III. For example a weak optical signal modulated by a voice would produce a signal of constantly varying frequency. The techniques discussed below that work well for detecting a repeating waveform would generally fail for such a signal. Other approaches, such as using wavelet transforms, might be useful in detecting such variable frequency signals.

This paper describes one method of searching for Type III signals. A time-series measurement of starlight is transformed into a power spectrum using standard FFT techniques. This power spectrum is then searched for any small signal that rises above the background noise. A single-frequency tone (sine wave) will generate a single peak in this spectrum. A more complicated periodic waveform will be decomposed in the spectrum into its Fourier components (harmonics), which will appear as a series of equally spaced tones. This method can be used to efficiently cover wide range of frequencies, depending on the time resolution of the input data series. It does have the limitation of requiring that the frequency of signal remain essentially fixed during an observation, but once this condition is met, it provides a powerful method for finding small signals hidden in time-series data.

It should be noted that this approach is not new. After the discovery of pulsars by Bell & Hewish in 1968 [15], there was great interest in finding additional pulsar candidates by searching radio-frequency power spectra for weak, repetitive signals. The recently-developed Fast Fourier Transform helped expedite these searches by dramatically reducing the computer time required for calculating a transform. Despite this improvement, many of the papers of that era reflect the need to optimize searches in a way that minimized the number of computer cycles required [16]. When a simple addition took 5μs to perform, the idea of calculating 50,000 1024-point FFTs to form a single power spectrum was probably not considered seriously. But with the dramatic increases in computer capability over the intervening years, such concerns are now of secondary importance. Conclusions from that earlier era, based on the very real computer constraints of the day, must not be allowed to bias our thinking now that those constraints have largely been removed.

Much of this paper is concerned with establishing how small a signal can be detected by searching power spectra. To accomplish this, a number of single frequency tones are added to a variety of measured star data, and the detection of those tones quantified in terms of the SSNR measured in the spectrum. A three-channel photon counting instrument, coupled with a 30" (0.76m) telescope provides the star data for this analysis. These data automatically incorporate realistic photon counting statistics and the effects atmospheric scintillation into the results. §2 describes this instrument, its data output and standard analyses performed. §3 shows an example of using the power spectrum approach to detect the Crab Pulsar against a high level of background light, and §4 presents key analysis results. The discussion in §5 considers related topics, such as methods for enhancing a weak detection. Summary conclusions are listed in §6.

2. System Description

2.1 Instrument

The instrument used to provide data for these simulations is shown schematically in Fig 1, and its main components listed in Table 1.

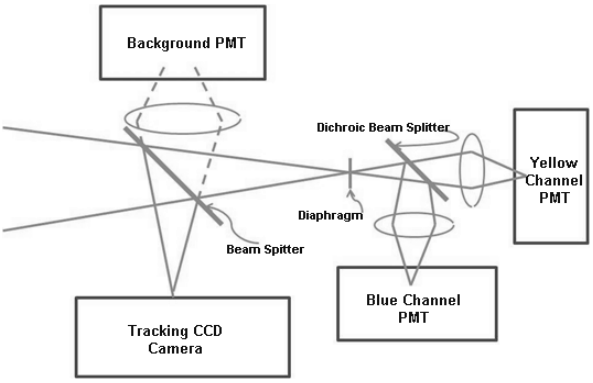

Fig. 1–Schematic of Triple Photometer. Note that the diaphragm is reflective to improve detection of background light

Hamamatsu photon counting modules were chosen for their low dark rates (typically <100/s), high linearity (to 2.5×10^6/s), and ease of operation (single 5V input).

Table 1—Triple Photometer Components

Telescope	0.76m	Big Bear, CA
PMT Modules	H8259-1,-2	Hamamatsu
Counter	DAQ 6602	National Inst.
Dichroic mirror	50%@510nm	Edmund Optic

Photon counts are recorded in simultaneous samples for each of three channels: two separate color bands (Y & B), and a broad-band measurement of background sky light. The background channel detects "signals" in the light surrounding the target star from clouds, airplanes, lightning, nearby lights, etc., and has proven to be essential for eliminating such spurious signals from the analysis. Fig. 2 shows the three photon counting photomultipliers configured for operation with the 30" telescope.

2.2 Data Handling

All data used in this study were accumulated with a standard set of parameters (Table 2). Photons counts from each the three photomultiplier tubes are accumulated with timing driven by a single 20,000Hz clock. This produces three time series of raw 50μs data sampled simultaneously. A fourth "white light" series can be formed by adding the two color channels together. The duration of an observation can be of any length, but is fixed at 2400s for all data used here.

Fig. 2- Triple Photometer at prime focus

Table 2 Parameters for Standard Observation

Duration	2400s
Sample Rate	20,000/s
Data Format	Integer photon counts
Data Volume	3x4.8x10^7 samples
Bin Levels	4x to 4096x
Power Spectra	1024 point FFT

Each raw time series is repeatedly re-binned by a factor of 4, forming new series with samples 200μs, 800μs,…204.8ms long. Each of these new series is converted into a ***power spectrum*** covering frequencies from zero to the Nyquist limit for that series. The resulting power spectra are then searched for signals too weak to be seen in the time-series data.

Note that for a typical observation lasting 40 min, there is sufficient data to form a large number of power spectra for each bin level. For example, with 4.8x10^7 samples of raw data, 46,898 power spectra (1024 point, 50% overlap) can be formed. Adding these spectra together reduces the background noise relative to a single spectrum by a factor of 216, a dramatic improvement. While this gain is less for higher bin levels, it is still results in a significant reduction in background spectral noise (Table 3).

Table 3-Properties of Binned files & Spectra

Bin Level	# of Points (Y, B)	Spectra Range (Hz)	# Spectra Summed	Bkd Noise (dB)
raw	48,000,000	10,000	46,898	0.022
1	12,000,000	2,500	11,723	0.044
2	3,000,000	625	2,930	0.085
3	750,000	156.25	731`	0.171
4	187,500	39.1	182	0.34
5	46,875	9.77	44	0.69
6	11,719	0-2.44	10	1.47

3. Crab Nebula Pulsar

Before addressing the limits found with this approach, it is instructive view the well-known source of modulated light: the Crab Pulsar (PSR B0531+21). Time series data for an observation on March 31, 2017 are shown in Fig. 3, with Y the upper trace, B in the middle and sky background at the bottom.

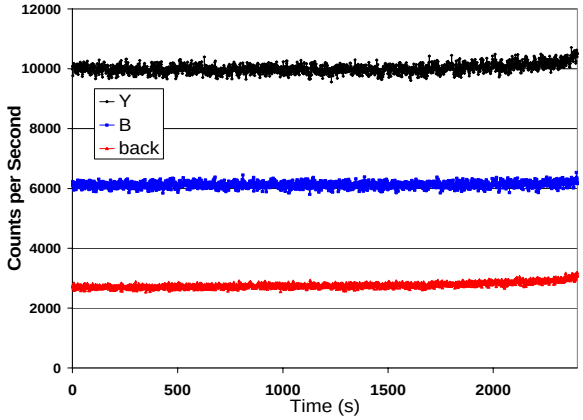

Fig. 3 Time-series of Crab Nebula + pulsar

One would normally make this observation on a moonless night with a very small diaphragm to exclude as much light from the nebula as possible. But in order to illustrate this use of power spectra, this observation was made with a large 27arcsec diaphragm on a moonlit night. The total signal levels (Y~10,000, B~6,000 counts/s) include light from (1) the Crab nebula (~50% of the total), (2) background skylight and moonlight (~45%), (3) a nearby star (~4%) and the Crab Pulsar (~1%). The pulsar is known to produce a precisely repeatable light "signal", but its presence is lost in noise for any time-series display of this data, regardless of time resolution.

In contrast to the time-series, the pulsar can be easily found in the power spectra, even if one had no advanced knowledge of its frequency or even its existence (Fig.4). The background noise in this plot (0.17dB) results from adding 731 individual power spectra together as seen in Table 3. This noise level is much smaller than the signal from the pulsar, allowing the fundamental and several harmonics to be clearly seen.

Once the resonance in Fig. 4 is found, the frequency of the fundamental can be measured (~29.6Hz) and used to extract the waveform by adding photon counts from each of the 71,000 pulsar rotations together. The resulting waveform (Fig. 5) is displayed with 0.5ms resolution. The vertical scale for this figure has been calculated to show the average number of photons detected during ***a single*** rotation of the pulsar.

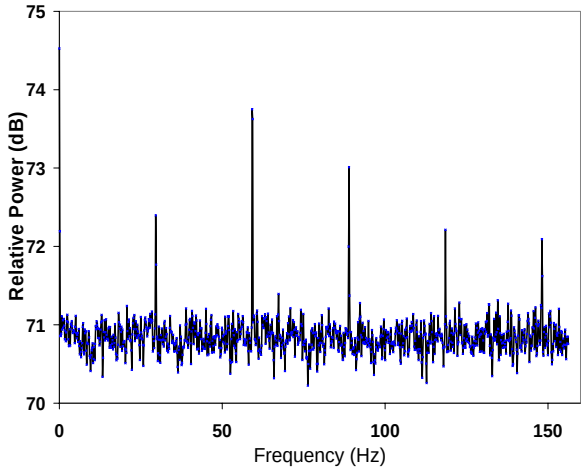

Fig. 4 Crab pulsar Power Spectrum (B channel)

The peak number of pulsar photons recorded during each rotation (0.32) can be compared with the average background during the same interval (~3 photons per 0.5ms) giving an example of the detection of a weak signal against a background that is 9 times stronger (RSA=1/9). Note that if this factor instead measured ratio to the average signals (pulsar = 55/s, background= 6,000/s) the ratio would be ~1/100. Since the peak-to-peak value seems better correlated with observed ssize of spectral peaks, this parameter is used in the definition of Relative Signal Amplitude.

Without any advanced knowledge the Pulsar characteristics, the power spectrum has clearly revealed a signal that could not be detected in the time series alone. Peaks in the power spectrum stand out clearly with a signal-to-background noise ratio of roughly 17. This suggests that significantly weaker signals could have been found had they been present in this data.

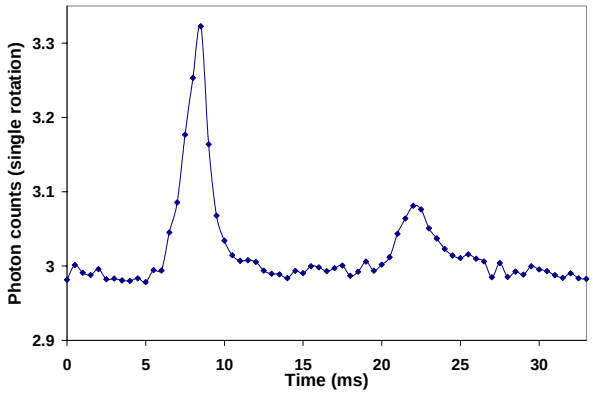

Fig. 5–Average light curve for 71,000 rotations of the Crab pulsar (B channel) during a 40min observation

4. Signal detection limits

4.1 Simulation Approach

Just how small a signal can be detected using this approach? This question is addressed by adding several weak sine waves to existing star data and examining the power spectra of these altered series. In order to focus on key parameters affecting the detection of these signals, several variables are fixed: (1) each "observation" is 2400s long, (2) each added signal "tone" is a pure sine wave [added as 1-sin(ωx)], (3) the same range of frequencies (Table 4) are added to each star data file and (4) the same processing steps, described above, are used to analyze the entire set of star data + tones. Table 5 lists typical stars, of brightness ranging from 10^3 to $2x10^7$counts/s, used in this analysis.

Table 4 Inserted tones

Bin Level	Inserted Tone (Hz)	Position in Spectrum
0 (raw)	6,689	686 of 1024
1	1,100	452
2	355	583
3	100	656
4	21	552
5	5	525
6	1.4	588

This approach allows the analysis to focus on the three variables that determine whether or not a signal is detected. These are (1) the peak-to-peak signal intensity, (2) the frequency of the added wave and (3) the brightness of the background star itself. The intensity of the input signal is expressed as a fraction, the RSA.

The addition of small signals to the existing photon count data must be carefully done. All measured star data are ***integer*** photon counts per sample. All added signals must also be integer counts. If the simulation calculates that 1/100 of a photon should be added to a particular time sample, this fraction cannot be ignored, but must be translated into an integer photon count value. To accomplish this, the simulation calculates a random photon level to be added each 50μs time sample of the raw data file, based on the fractional photon value calculated for all tones added to that sample.

A Poisson random number generator [17] is used to calculate the number of photons to add for each sample. Since the calculated fractional photon value is always small (usually less than 1), a Poisson generator is the appropriate choice. Like all random number generators, this generator is not perfect. But extensive testing (10^7trials/case) showed that the number of photons generated closely matches calculated probability over almost the entire range of expected fractional signals

(0.005 to ~4 photons). For very small values (<0.002 photon) the generator seemed to underestimate the correct value, but this had little affect on the simulated waveform. While this testing gave good confidence that the statistically correct signal was being added at each point, further confirmation was achieved when the shape and amplitude of the added waveforms was examined directly using waveform folding techniques.

Table 5 Typical star data used in for tone simulations

Star	Y (/s)	B(/s)	Backgnd(/s)*
Crab Neb*	10,013	6,125	2,773
M67-1221	31,927	13,641	2,032
HIP65407	104,188	63,739	1,864
HD101364	185,001	134,200	3,552
HD129357	408,851	303,968	849
Sun1*	921,925	4,014,603	1,564,897
Sun3*	4,210,768	12,164,024	16,374,792

*Not all "star data" were stars: The Crab nebula and various sky background time series were used as "faint stars". The "Sun" signals are the sum of several sunlight time-series. These "stars" have the lower scintillation levels expected for large telescopes [18].

4.2 Power spectra results

Once the small signal tones are added to the time-series data, power spectra are calculated for each bin level and displayed stacked on a single graph (Fig. 6). Each spectrum has been offset vertically from the raw data spectrum (lowest curve) for clarity. The lowest spectrum covers the frequency range from 0 to 10,000Hz, the next one up covers 0 to 2,500 Hz, etc. The background noise for the raw spectrum has been reduced to the point (by adding together 46,898 individual spectra) that it is invisible at this scale. As the bin level increases, the number of available data points decreases, resulting in the increasing noise level as one moves from the bottom curve to the top. Fig. 7 brings out details of the two lowest curves in Fig. 6 using a greatly expanded vertical scale.

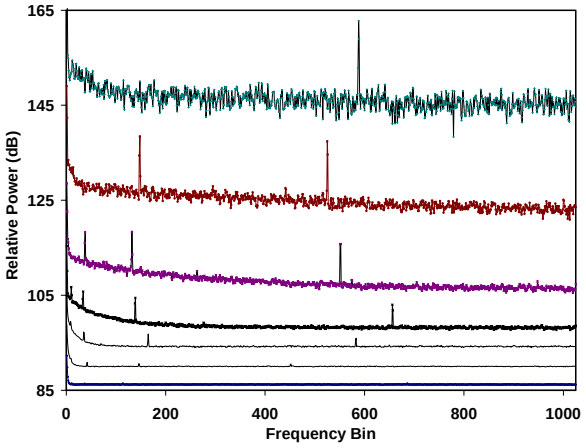

Fig. 6 Typical power spectra of a star (HD101364) with tones added for the 7 frequencies in Table 4.

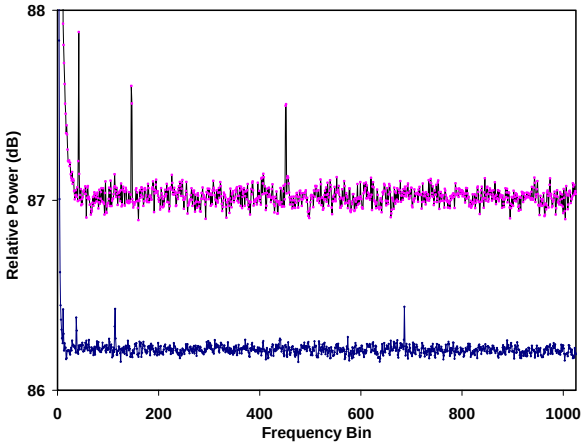

Fig. 7 Two lowest power spectra in Fig. 6 at expanded scale

In the following analysis the Spectrum Signal/Noise Ratio (SSNR) is used to measure visibility for every spectral peak. Although it is often possible to find peaks in the power spectrum with an SSNR less than 5 (particularly when the location of the peaks is known *a priori*), a SSNR value of 5 is defined here as the minimum detectable signal.

4.3 Detection vs signal frequency

Signals were generally detectable over the entire range of inserted tones (1.4 to 6689 Hz). But as can be seen in Fig. 8, the SSNR of peaks for two highest frequencies (1100 and 6689Hz) were typically smaller than for peaks of lower frequency with the same RSA. A similar reduction is seen for the lowest frequency. While the low frequency roll-off might be due to the increasing power of atmospheric scintillation, the reduction at high frequencies is harder to explain. The lowest curves of Fig. 8 illustrate typical responses to near-threshold signals, showing that the highest frequencies (>100Hz) have generally disappeared, while the lowest (1.4 to 21Hz) are clearly seen. This behavior is typical across a broad range of star intensity-- higher frequency signals tend to disappear first as the RSA is reduced.

4.4 Detection vs RSA

Fig. 9 plots the measured SSNR of detected tones as a function of RSA and the intensity of the host star count rate. For example, the middle dashed curve is generated with signals of RSA=1/316. If the host star produces 10^6counts/s (50 counts per 50μs sample) the peak-to-peak amplitude of each of the seven added tones is 50/316 = 0.158 counts per sample. The curve shows that these added signals produce an average peak

of SSNR~15 in the power spectrum, making them readily detectable at all frequencies except possibly the highest (6689Hz).

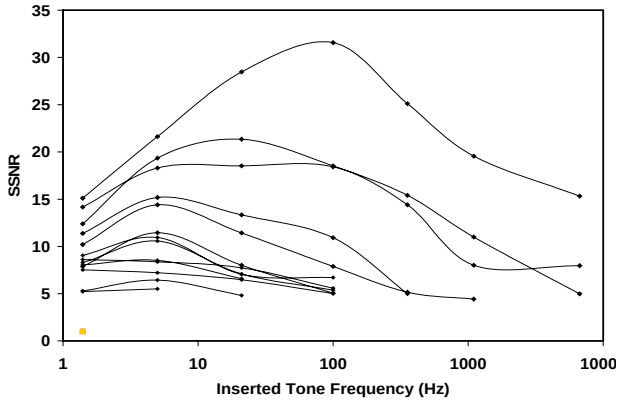

Fig. 8 Variation of SSNR vs frequency for curves of constant RSA

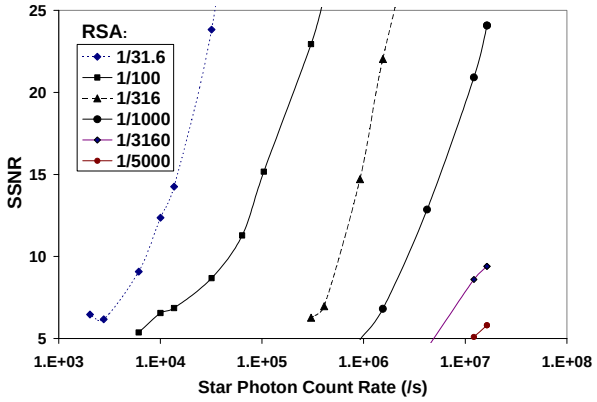

Fig. 9 Tone SSNR vs RSA and host star brightness

A few observations should be made regarding these curves. First, the SSNR for a given RSA is strongly dependent on the brightness of the host star. The brighter the star, the easier it is to detect small added signals. This implies that it should be possible to verify a suspected ETI signal using a larger telescope or a longer observation.

Second, the SSNR values plotted are usually the average of the 4 or 5 largest values over the signal frequency range. As seen in Fig.8, this is often reduced to 2 or 3 available values for the very weakest signals. This may explain the tendency of the curves to bend at the lowest values of SSNR.

Third, the curves cut off at$1.6x10^7$/s since this is the largest star rate available for this analysis (Table 5). There is every reason to believe that the trends shown here will continue for even larger star count rates.

The conclusion evident from Fig. 9 is that the smallest signal that can be detected by examining power spectra depends strongly on the apparent brightness of the host star itself. This conclusion is quantified in Fig. 10 which plots RSA value producing a threshold peak (SSNR=5) vs the count rate measured for the host star. This plot suggests that, over a wide range of star signal intensity, one can reasonably expect to detect a tone signal with an amplitude of approximately the square root of the star count rate (s^{-1}). Thus, finding a signal that is 10^4 times weaker than the brightness of the host star requires a star rate of roughly10^8 counts/s.

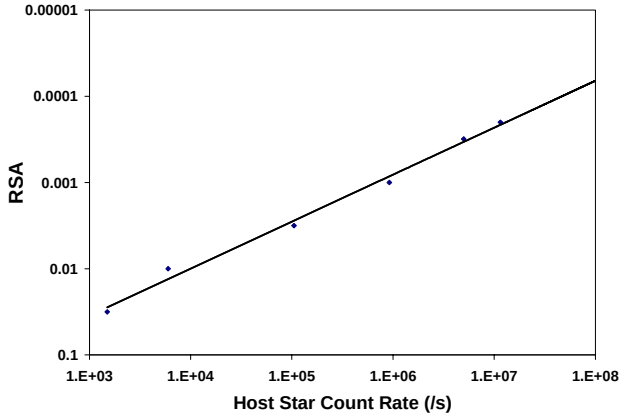

Fig. 10 Minimum detectable RSA vs host star count rate

4.5 Other Signals

Of course there is no expectation that any ETI signal will be a pure sine wave. Fig. 11 shows a schematic of a negative square wave pulse that repeatedly blocks 1/1000 of a star's light 20 times per second (lower curve), and the resulting power spectrum. Since this pulse is "on" only 10% of the time, the peaks produced in the power spectrum are smaller (~half) than the peak for a sine wave of the same amplitude.

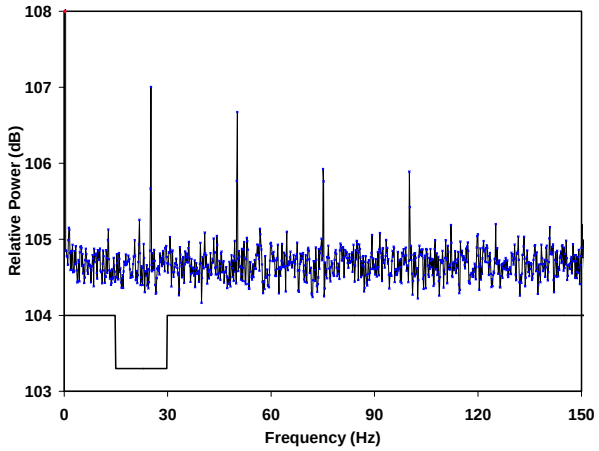

Fig. 11 Spectrum of negative square pulse

While the power spectrum provides a fast, sensitive means of finding frequencies present in time-series data, deeper searches are possible using other means. Figs. 12 and 13 illustrate this for an added tone of RSA = 1/5000 and frequency =100Hz. Fig. 12 shows that no trace of this signal is visible in the power spectrum at 100Hz. But since we know the exact frequency of the missing tone, the entire time-series data can be searched for this exact frequency by folding 120,000 20ms segments together. The result of this process is plotted

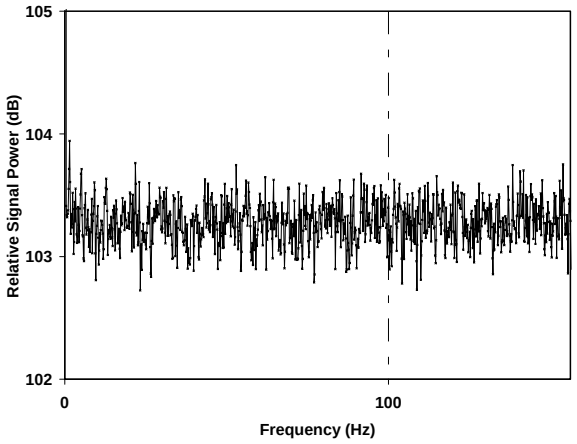

Fig. 12 Power spectrum of weak 100 Hz signal (RSA=1/5000)

Fig. 13, which clearly shows that a 100Hz signal is present in the data. The missing signal is not only detected, but its peak-to-peak amplitude can be estimated, giving a measured RSA of ~1/5600. Considering that the amplitude of the input tone was only 0.121 photons, and every one of the 48 million data samples went through a Poisson generator to produce an occasional added photon count, Fig. 13 gives excellent verification of the validity of the simulation process.

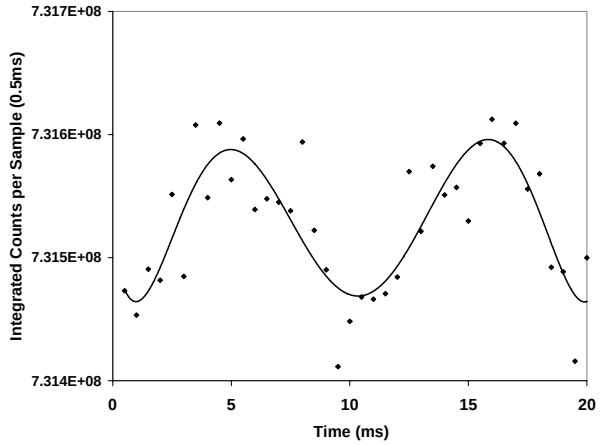

Fig. 13 100Hz signal not detected in Fig. 12

Another verification of the analysis is provided by "real" signals that occasionally appear in power spectra. Fig. 14 adds four specific cases to the simulated tone data in Fig.9. First, the Crab pulsar detection is plotted as an example of a strong signal easily detected in a weak host "star". As discussed in §3, the pulsar signal had an RSA of ~1/9. Second, the spectra peak produced by the square wave in Fig.11 is also plotted. The arrow indicates that the measured SSNR is substantially lower than measured for a pure sine wave. In this case, the low duty cycle of the pulse (10%) shows up as a much smaller spectral peak than a sinusoidal tone of the same amplitude.

Two "signals" that appeared during routine observations are also plotted in Fig. 14. The first, marked 15.1Hz was due to an unexpected vibration in the telescope. It caused a lot of early excitement a couple years ago when it appeared in an observation of Cyg X-1 [19]. It was finally identified as an instrumental effect when a weak 15.1Hz resonance was seen in observations of other stars. The RSA measured for this "signal" was ~1/85, reasonably consistent with its position near the 1/100 curve. The last point was almost certainly caused by a 371Hz light leak (computer?) somewhere in the observatory during an observation of HD195034 (Fig. 15). Its measured RSA value (~1/300) is clearly consistent with its location on Fig.14. Repeated observations of HD195034 have failed to reproduce this signal. For each of the three signals detected in the power spectra the measured SSNR and RSA values are consistent with values predicted by Fig. 9.

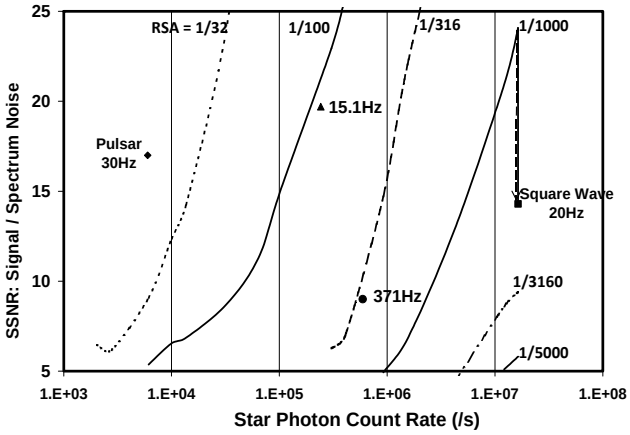

Fig. 14 Same data shown in Fig. 9 with three "real" signals added, plus a simulated square wave.

5. Discussion

5.1 Use of multiple PMTs

None of these results have touched on the very real limits of traditional photon counting when exposed to very large count rates. The excellent noise and linearity of these sensors generally extends to count rates of less than $5x10^6$/s, at which point dead-time limitations

become important. This implies that a total count rate of 10^8/s could be achieved if the starlight is shared between at least 20 tubes. An instrument designed to partition starlight between this many tubes should not be particularly challenging to make. A fiber optic beam splitter could be used to effect this partition [13]. If a series of dichroic beam splitters were used, the system could provide spectral discrimination for any narrowband signal. Adding all the spectral time-series together would produce a time-series that could be used to detect white light variations a factor of 10^4 below the incident starlight intensity.

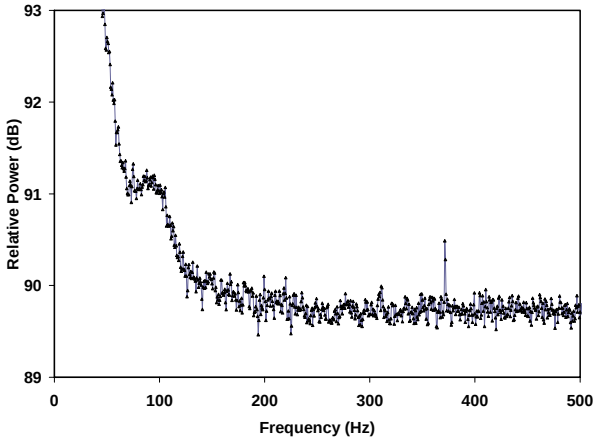

Fig. 15--A 371Hz "signal" in spectrum of HD195034 plotted in Fig. 14. The increase in background power at low frequencies is due to atmospheric scintillation

5.2 Detection vs star magnitude

The Triple Photometer in conjunction with a 30" telescope records about 600,000 white light counts (Y+B channels) per second for an 8th magnitude star. This translates into V=4.9 and V=2.4 for 10^7 and 10^8 counts/s, respectively. Larger telescopes will reach these count rates for significantly fainter stars (e.g. V=9.0 and 6.5 for a 5m telescope). A larger aperture also has the advantage of suffering less from power added by atmospheric scintillation [16]. As is evident in Fig. 15, the scintillation due to atmospheric turbulence can significantly increase the background power spectrum level at low frequencies.

5.3 Increasing sensitivity to a weak signal

There are several ways of increasing SSNR once a threshold signal is suspected. First, longer observations reduce background spectral noise, thereby increasing the visibility of a detected feature, assuming that the signal is present throughout the longer observation. In the extreme case, observations taken over several nights could be combined. Second, if the suspected signal occurs in only one color channel, adding an appropriate spectral filtering should also increase the SSNR of the detected feature. Clearly, using a larger telescope should also help, assuming that the PMTs used can handle the increased signal. As seen in Fig. 9, even a relatively small increase in the host star count rate can significantly increase the detected SSNR.

While the above steps would enhance subsequent observations, the wait for the next clear night might be significant. In the meantime the original data can be searched in the time domain as was illustrated for Fig. 13. If a signal can be seen in the folded time series, its evolution during the entire observation could be traced to discover any variations that might have occurred.

6. Conclusions

The data and simulations presented here lead to several important conclusions:

(1) Power spectra of time-series star data provide an excellent tool for finding weak embedded signals.

(2) Detection with this method relies on the signal having a constant frequency, not on knowing that frequency or waveform shape in advance.

(3) The signal can be either positive (e.g. a laser light) or negative (periodic starlight obscuration).

(4) Signals can be found over a large frequency range, limited mainly by the time resolution of the input data

(5) As brighter stars are observed, weaker signals can be detected (measured as a fraction of the star count rate)

(6) A signal 10^4 times fainter than the host star should be detectable for a bright star producing ~10^8 photon counts per second.

(7) Although atmospheric scintillation can add significant power to the low frequency end of a power spectrum, the lower frequency signals (1.4 to 20Hz) seem unaffected, and are the last to disappear as the Relative Signal Amplitude decreases.

How do the signal levels in Figs. 9 & 10 translate to transmitted power level? A distant ETI source would need to transmit significantly less power if modulated for us to detect. Using a 10m telescope to transmit a 550nm laser beam, the signal will appear $3.5x10^{15}$ times brighter than for an isotropic source [9]. If a star with the sun's output power is viewed with a photometer capable of detecting modulated signals a factor of 10^4 fainter than the star, the transmitted power needed would be $3.8x10^{26}/(3.5x10^{15}*10^4) = 10^7$watts. While this is still a significant power level, the gain achieved by modulation might be important to the transmitting extraterrestrials.

On the other hand, suppose that the extraterrestrials have constructed a means to modulate their home star's

light. Perhaps several large structures with mechanical or liquid crystal modulators could be used. Depending on the implementation details, this signal would spread over a substantial solid angle of the star's emission. It's certainly conceivable that the transmitting ETI may not even know or care about us. Perhaps we would simply be eavesdropping on communications broadcast to their space fleet or colleagues across the Galaxy!

Acknowledgements
The author sincerely thanks Claude Plymate for his review of the manuscript and many helpful critiques and suggestions.

References

[1] F. D. Drake, How can we detect radio transmissions from distant planetary systems? Sky & Telescope, 19 (1960), 140.
[2]R.N.Schwartz, C.H.Townes, Interstellar & Interplanetary Communication by Optical Masers, Nature, 190 (1961), 205.
[3] E.J.Korpela, et al, Status of the UC-Berkeley SETI Efforts, Proc. SPIE 8152 (2011), 894066.
[4] J. Maire, S.A.Wright, et al, A near-infrared SETI experiment: Commissioning, data analysis, and performance results, Proc. SPIE 9908 (2016), 990810, (12p).
[5]S.K. Mankevich, E.P.Orlov, Interstellar laser communication: implementability, criterion and optimisation conditions for the addressed signal search and sending, Quantum Electronics, 46(10) 966-971 (2016).
[6] R. Bhathal, Optical SETI in Australia, Proc. SPIE 4273 (2001), 144-152.
[7]A.W. Howard, P. Horowitz, D.T. Wilkinson, et al. Search for nanosecond optical pulses from nearby solar-type stars, ApJ 613 (2004), 1270.
[8] A.U.Abeysekara, et al., A search for brief optical flashes associated with the SETI target KIC8462852, ApJL 818:L33 (2016), (6pp).
[9] M. Schuetz, D.A.Vakoch, S.Shostak, J.Richards, Optical SETI observations of the anomalous star KIC8462852, **Ap**JL 825:L5 (2016), (5pp).
[10] N.K.Tellis, G.W.Marcy, A search for optical laser emission using Keck HIRES, PASP 127(2015), 540-551.
[11]N.K.Tellis, G.W.Marcy, A search for laser emission with megawatt thresholds from 5600 FGKM stars, AJ 153 (2017), 251.
[12]E.F.Borra, Searching for extraterrestrial intelligence signals in astronomical spectra, including existing data, ApJ 144 (2012), 181-187.
[13]W.R.Leeb, A.Poppe, E. Hammel, et al. Single-photon technique for the detection of periodic extraterrestrial laser pulses, ASBio 13(2013), 521-535.
[14]L.F.A.Arnold, Transit light-curve signatures of artificial objects, ApJ 627 (2005), 534-539.
[15] A. Hewish, S. J. Bell, J.D.H. Pilkington, P.F. Scott, T.W. Cole, Observation of a Rapidly Pulsating Radio Source, Nature 217 (1968), 709-713.
[16] W.R. Burns, B.G. Clark, Pulsar Search Techniques, A&A 2 (1969), 280-287.
[17]J.D.Cook, Generating Poisson random values, 14 June 2010, https://www.johndcook.com/blog/2010/06/14/generating-poisson-random-values/
[18]A.T.Young, Photometeric error analysis VI. Confirmation of Reiger's theory of scintillation, AJ 72 (1967), 747.
[19] R.H.Stanton, Triple Photometer: Design and Initial Results, Proc. 34th Annual Symposium on Telescope Science, Ontario, CA, (2015), pp. 69-77.

.